Pergamon

Int. J. Heat Mass Transfer. Vol. 40, No. 10, pp. 2393–2406, 1997

0017–9310/97 $17.00+0.00

PII: S0017–9310(96)00292–X

Post-nucleation growth of water microdroplets in supersaturated gas mixtures: a molecular simulation study

V. P. CAREY, S. M. OYUMI and S. AHMED

Mechanical Engineering Department, University of California, Berkeley, CA 94720-1740, U.S.A.

(*Received* 7 *March* 1996 *and in final form* 26 *July* 1996)

Abstract—Prediction of heat and mass transfer during post nucleation growth of liquid microdroplets in a supersaturated mixture of vapor and non-condensable gas is difficult because in the early stages of the process, the droplet size is usually comparable to the mean free path of the surrounding gas molecules. Transport then falls in the transition regime between free molecular flow and continuum transport. In the study reported here, a direct simulation Monte Carlo (DSMC) scheme was used to model the molecular transport during quasi-equilibrium condensation growth of water microdroplets in supersaturated mixtures of water vapor and a non-condensable gas. A new treatment of the boundary conditions at the droplet interface is proposed which properly accounts for the energy and mass balance at the interface as well as thermodynamic requirements that must be imposed there. This treatment makes it possible to predict the initially unknown droplet interface temperature as part of the simulation calculation. Predictions of this scheme for water–argon mixtures are shown to agree closely with measured droplet growth rate data. Simulation results are also presented for mixtures of water vapor and nitrogen. The effects of varying droplet size and ambient concentration on transport are explored in detail for microdroplet condensation in the transition regime.

INTRODUCTION

Condensation of liquid microdroplets in a supersaturated mixture of its vapor and a non-condensable gas is an important fundamental process in nature and in technological applications. Condensation growth of water microdroplets in the atmosphere immediately following nucleation is an important element of the microphysics of cloud formation in the atmosphere. Fog formation in air-conditioning evaporators and precipitation which results from supersaturated conditions in industrial process flows also fall into this category. For the initial stage of droplet growth in such circumstances, the size of the droplets is often comparable to the mean free path of the surrounding gas molecules. As the droplet grows, the heat and mass transfer associated with the process traverses the transition regime between free molecular and continuum transport. Since neither free molecular theory nor continuum theory is accurate in the transition regime, prediction of the condensation growth of microdroplets in this size range is particularly challenging.

Condensation growth of liquid droplets in a supersaturated surrounding gas has been the subject of numerous studies, spanning a variety of applications. The majority of these studies have focused on relatively large droplets, with diameters greater than 5 μm, surrounded by a gas at moderate pressures. The transport in such circumstances can be predicted by continuum theory.

There have been relatively fewer investigations of non-continuum effects on droplet condensation growth. In an early study, Kang [1] developed analytical models of condensation droplet growth in a mixture of supersaturated vapor and a non-condensable second gas. The analysis is based on a combination of elements from continuum theory and kinetic theory. The analysis considers condensation for a fixed droplet condition or a changing temperature resulting from the condensation energy transport. The droplet growth history was predicted from the analysis. Somewhat later, Sampson and Springer [2] used the moment method and a kinetic theory based approach to develop a prediction of mass flux during condensation of droplets in vapor–gas mixtures. The resulting relation for the mass flux can be used over the entire spectrum of droplet Knudsen number from free-molecular to continuum transport. At about the same time, Shankar [3] also used the Maxwell moment method to derive relations for the mass and energy flux to a droplet growing by condensation in a mixture of its vapor and an inert gas. A kinetic-theory-based analysis of droplet condensation growth was also developed by Gajewski *et al.* [4]. These investigators generated predictions of the heat and mass transport by using a numerical method to solve the full nonlinear BGK model equation. Lou [5] explored the differences between infinitesimal and finite temperature difference on the condensation growth rate of droplets using a kinetic theory formulation and the four moment method.

NOMENCLATURE

c_p	specific heat at constant pressure
c_v	specific heat at constant volume
D_d	diameter of droplet
D_m	effective diameter of molecules
D_v	mass diffusion coefficient in vapor
h_{lv}	latent heat of vaporization
j	molecular number flux
k_v	gas thermal conductivity
k_B	Boltzmann constant
m	mass of a molecule
n_m	number density of molecules
P	pressure
q''	energy flux
r_d	radius of droplet
R	ideal gas constant
$\Re$	a random number uniformly distributed on [0, 1]
T	absolute temperature
$\hat{u}_{lv}$	latent energy per water molecule merged into droplet
$\mathbf{v}_r$	relative velocity vector for collision pair
X_w	mole fraction of water vapor in gas mixture.

Greek symbols

α	thermal diffusivity
Δt	time interval for one time step of simulation
ε	molecular energy component
λ	molecular mean free path
ρ	density
σ_{lv}	liquid–vapor interfacial tension
σ_t	energy accommodation coefficient.

Subscripts

d	corresponding to the liquid droplet surface
em	corresponding to particles emitted by the droplet
in	corresponding to particles incident on the droplet
l	liquid
rot	rotational
tr	translation
v	vapor
∞	corresponding to far ambient conditions
0	corresponding to conditions in the gas adjacent to the droplet surface
4	corresponding to $r/r_d = 4$.

More recent investigations by Loyalka [6], Lang [7], Chernayak and Margilevskiy [8] and Young [9, 10] also explored analytical extensions of kinetic theory as means of predicting heat and mass transfer between a condensing droplet and a surrounding gas at arbitrary Knudsen numbers. Widder and Titulaer [11] formulated an analysis of transport to a condensing droplet in a supersaturated mixture of a light non-condensable gas and a heavy vapor species. Their analysis was constructed in terms of the Navier–Stokes equations and the Klien–Kramers equation for Brownian motion of the vapor molecules. The governing equations were solved numerically to predict the droplet temperature and growth rate for specified ambient conditions.

All previous efforts to analyze droplet condensation under transition regime conditions have apparently been based on analyses using kinetic theory. An alternate approach is to use a molecular simulation model. This type of approach has been used by Carey and Hawks [12] to model evaporation of nitrogen microdroplets in pure superheated nitrogen gas. It has also been used by El-Afify and Corradini [13] to model low pressure transient condensation of mercury vapor on a vertical flat surface. In a subsequent paper, El-Afify and Corradini [14] extended their simulation model to transient condensation of mercury vapor on a flat vertical surface in the presence of a monatomic non-condensable gas. The present investigation differs from these in that we are interested in condensation growth of a spherical droplet in a supersaturated binary gas mixture containing the condensing vapor and a non-condensable gas. Our objective was to develop a model that is applicable to condensation of water microdroplets in the atmosphere and in other technological applications where condensation of microdroplets occurs in the presence of one or more non-condensable species.

Droplet condensation in a supersaturated gas is fundamentally different from the process of condensation on a flat surface studied by El-Afify and Corradini [13, 14]. These investigators considered condensation in the absence of forced or free convection. Except for the limiting case of free molecular transport in the surrounding gas, condensation on a flat surface is an intrinsically time-varying process in which the thermal and mass concentration layers in the gas grow progressively thicker with time. In contrast, for any specified supersaturated ambient conditions, steady temperature and concentration profiles are established in the gas for condensation on a spherical droplet of fixed size.

For most circumstances of interest, the size of the droplet increases significantly during the condensation growth over a time interval that is relatively long compared to the time required to achieve steady temperature and concentration fields in the surrounding gas. In such circumstances, the transport in

the gas at any instantaneous radius r_d during the droplet growth is well approximated by the steady state quasi-equilibrium transport that results from a droplet of fixed r_d condensing at the specified ambient conditions.

The microphysics of condensation in the presence of a non-condensable gas is significantly more complex than condensation of the pure vapor phase of the liquid in the droplet. Condensation removal of vapor at the droplet interface and mass diffusion result in a water vapor concentration at the interface which can be significantly different from that in the far ambient. For a quasi-equilibrium process, the interface temperature must equal the saturation temperature of the liquid species at the partial pressure of the vapor in the gas at the interface. Thus the droplet surface temperature cannot be specified *a priori*. Any transport analysis scheme for this type of droplet condensation process must therefore include a means of determining the interface temperature as an integral part of the analysis. Also, to handle an arbitrary mixture, treatment of molecules that store energy by rotation as well as translation must be incorporated into the model.

Two conditions must be satisfied for the quasi-equilibrium model to accurately predict transport at any instant during the droplet growth process. First, the time scale associated with internal conduction inside the droplet must be small compared to the characteristic time associated with transport in the gas. Since the liquid thermal conductivity is large compared to that of the vapor, this condition is satisfied for the systems of interest here. This line of reasoning implies that the temperature is essentially uniform within the droplet but may vary slowly with time as the droplet grows. In addition, the quasi-equilibrium model treats the radius as fixed during the simulation, even though the droplet is actually growing during the condensation process. This is a good approximation if the characteristic time of the droplet growth process $(r_d/(dr_d/dt))$ is large compared with the characteristic time for transport in the gas. This requirement is met for the systems studied here. The droplet size changes significantly over milliseconds while times on the order of microseconds are required to establish steady transport in the gas.

The investigation summarized in this paper used a stochastic, Monte-Carlo direct-simulation scheme as a method for predicting the molecular transport to a condensing microdroplet in the presence of a second non-condensable species. The simulation was specifically applied to microdroplets condensing under transition regime conditions. This study appears to be the first to apply a direct-simulation Monte Carlo method to condensing microdroplets for circumstances in which non-continuum effects are important. The simulation method used in this study is similar to that used by Carey and Hawks [12] with modifications to account for condensation and to allow determination of the initially unknown temperature at the droplet surface.

The accuracy of the new treatment of the droplet surface condition used in this study was assessed by comparing its predictions with previously obtained data for droplet condensation in supersaturated argon–water gas mixtures. The simulation was also used to explore the effects of varying ambient water vapor concentration and droplet size on transport.

APPLICATION OF THE PARTICLE SIMULATION METHOD

The particle simulation method used here is a derivative of the direct-simulation Monte-Carlo (DSMC) technique pioneered by Bird [15]. Some of the refinements developed by McDonald [16] and Baganoff and McDonald [17] have also been incorporated into the scheme used here. The main features of the particle simulation method are described briefly in the Appendix. The special features added in our investigation to model the condensation growth of a spherical droplet in a supersaturated mixture of vapor and a non-condensable gas are described in detail below.

To minimize memory requirements and computational time, the simulation domain was limited to one octant around the droplet, as shown in Fig. 1. In addition, to avoid the computational costs of extending the simulation out to large radial distances, in this study the simulation domain was limited to a radial distance of four sphere radii, and the simulation boundary condition was matched to the continuum transport solution beyond $r = 4r_d$.

The temperature and water vapor concentration gradients decrease rapidly with distance from the sphere, approximately proportional to r^{-2}. Consequently, while the temperature may drop and the water concentration may rise significantly over a few mean free paths near the sphere, beyond $r = 4r_d$ it will take many free paths for the temperature or concentration to change significantly. The local Knudsen number $\lambda(dT/dr)/(T_d - T_\infty)$ decreases rapidly with distance from the sphere, causing the temperature and concentration profiles to approach those for continuum transport at large r. This line of reasoning, which divides the region near the sphere into a non-continuum region close to the body and a continuum transport region farther away was first used by Langmuir [18] to facilitate the analysis of non-continuum transport to a cylindrical body. The matching process proposed as part of our simulation scheme is therefore consistent with Langmuir's model which has been widely used for problems of this nature.

The octant simulation region shown in Fig. 1 was bounded by the surface of the sphere at $r = r_d$, the outer boundary at $r = 4r_d$ and specularly reflecting planar surfaces at $x = 0$, $y = 0$ and $z = 0$. The specular surfaces which lie along planes of symmetry have the effect of giving the octant the same statistical behavior as a complete sphere surrounded by particles. Each particle in the simulation represents

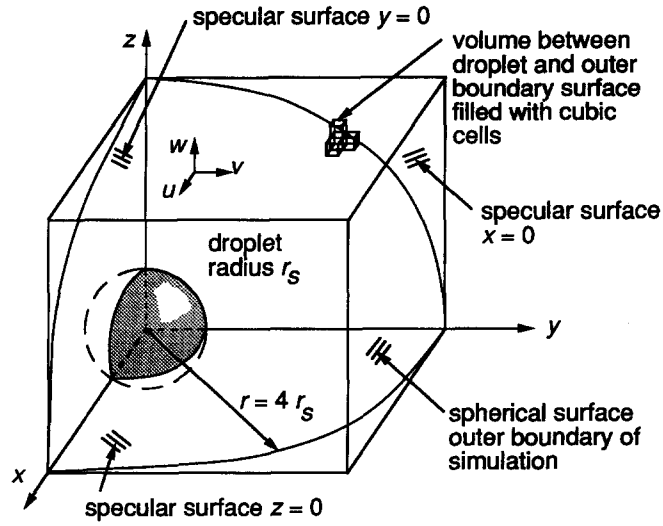

Fig. 1. Boundaries and cell grid for the simulation domain.

N_{mpp} molecules. The region bounded by these surfaces was filled with cubic cells which were used to collect collision candidate pairs and define regions over which particle properties were averaged to obtain macroscopic thermodynamic characteristics of the gas adjacent to the droplet.

Particles that move beyond the outer boundary when the particles are advanced along their trajectory were simply removed from the simulation. During each timestep, particles of each species are added to the simulation just inside the $r = 4r_d$ boundary. The rate of water particle addition $\dot{n}_w$ and the rate of nitrogen particle addition $\dot{n}_n$ are computed as

$$\dot{n}_w = N_{mpp}(\pi/2)(4r_d)^2 j_w \quad (1)$$

$$\dot{n}_n = N_{mpp}(\pi/2)(4r_d)^2 j_n \quad (2)$$

where j_w and j_n are the fluxes of water and nitrogen molecules across a surface predicted by kinetic theory for a mixture at a pressure P_∞, temperature T_4 and water mole fraction of $X_{w,4}$

$$j_w = \left(\frac{k_B T_4}{2\pi m_w}\right)^{1/2}\left(\frac{X_{w,4}P_\infty}{k_B T_4}\right) \quad (3)$$

$$j_n = \left(\frac{k_B T_4}{2\pi m_n}\right)^{1/2}\left(\frac{(1-X_{w,4})P_\infty}{k_B T_4}\right). \quad (4)$$

This treatment allows the simulation domain to establish whatever mean particle density is necessary to balance the inward and outward fluxes at the outer boundary. Equations (3) and (4) are derived from equilibrium kinetic theory. Implicit in their use here is the idealization that equilibrium Boltzmann distributions are valid at $r = 4r_d$. This idealization is justified because bulk motion of the gas induced by condensation at the droplet surface is small compared to mean molecular velocities, and because temperature and concentration gradients are low at this location.

Based on the observation that the liquid thermal conductivity is large compared to that of the vapor, conduction inside the droplet was idealized as being very fast. The temperature was therefore taken to be uniform within the droplet and transient conduction effects in the liquid droplet were not considered in the energy balance at the droplet surface.

When molecules from a surrounding gas enter the interfacial region near a solid or liquid phase, experimental evidence and molecular simulation studies indicate that only a fraction of the incident molecules thermally interact with the molecules of the condensed phase (see, for example, refs. [22–24]). It is generally acknowledged that the exact value of this fraction may vary from one system to another. In our simulations, this behavior is stochastically represented by specifying an accommodation coefficient σ_t which is taken to equal the fraction of incident molecules that thermally interact with the droplet surface.

If a particle strikes the droplet surface during a given timestep, a random number $\Re$ uniformly distributed on [0, 1] is compared to the specified accommodation coefficient. If $\Re > \sigma_t$, the particle is diffusely scattered from the surface. Its speed and rotational energy are left unchanged, but its direction is randomly set by sampling a distribution that, on the average, isotropically scatters particles from the surface. If $\Re \leqslant \sigma_t$, the particle interacts thermally with the surface.

Each thermally interacting particle is treated as if it merges into the liquid droplet, delivering its energy (including an energy of vaporization for water particles), to the droplet. Computationally, particles that merge into the droplet are removed from the simulation. The number of particles absorbed in this manner is counted, and the energy delivered to the droplet by these particles is summed.

In a subsequent portion of the timestep calculations, particles are added to the simulation domain just beyond $r = r_d$. Before executing the emission of particles from the droplet surface, the temperature

of the droplet surface is computed. Kinetic theory predicts that for an interface at equilibrium, the flux of emitted water vapor molecules is given by

$$j_w = \sigma_t \frac{P_{ve}(T_d)}{(2\pi m_w k_B T_d)^{1/2}}. \quad (5)$$

For the spherical microdroplets considered here, the equilibrium vapor pressure P_{ve} in the above relation is a function of the droplet temperature T_d and the droplet radius r_d

$$P_{ve} = P_{sat}(T_d) \exp\left(\frac{2\sigma_{lv}}{\rho_l r_d R T_d}\right). \quad (6)$$

In the above relation $P_{sat}(T_d)$ is the flat–interface saturation pressure for water at T_d. For the range of conditions considered in this study, surface tension effects on the saturation conditions were very small.

In the limit of long times, the steady-state energy exchange at the interface must satisfy conservation of energy

$$\sum_{i=1}^{N_{steps}} (E_{gain})_i = \frac{\pi}{2} r_d^2 j_w \Delta t \left(\hat{u}_{lv} + \frac{1}{2} k_B T_d\right) + 3 k_B T_d N_{mpp} \sum_{i=1}^{N_{steps}} (N_{non})_i. \quad (7)$$

In the above equation, $(N_{non})_i$ is the number of non-condensable molecules which thermally interact with the surface and then are re-emitted into the gas and $(E_{gain})_i$ is the energy delivered by molecules colliding with the droplet surface in time step i. The left side of the above equation is the total energy delivered by molecules colliding with the surface through N_{steps} time steps of the simulation. The right side is the energy carried away by molecules leaving the droplet surface. The first term on the right represents energy removed by water molecules, and the second represents energy carried away by non-condensable gas molecules re-emitted to the gas. Combining equations (5) and (6) and substituting into equation (7) yields

$$\sum_{i=1}^{N_{steps}} (E_{gain})_i = \frac{\pi r_d^2 \sigma_t P_{sat}(T_d)}{2(2\pi m_w k_B T_d)^{1/2}} \Delta t \left(\hat{u}_{lv} + \frac{1}{2} k_B T_d\right) \exp\left(\frac{2\sigma_{lv}}{\rho_l r_d R T_d}\right) + 3 k_B T_d N_{mpp} \sum_{i=1}^{N_{steps}} (N_{non})_i. \quad (8)$$

In equation (8), P_{sat} and $\hat{u}_{lv}$ are functions of temperature. For the purposes of our simulation calculations, P_{sat} was computed using the following relation which is a curve-fit to data for water between 10°C and 70°C based on the Clapeyron equation

$$P_{sat}(T_d) = e^{(A - B/T_d)}. \quad (9)$$

In equation (9), $A = 18.71$ and $B = 5240$ for T_d in K and P_{sat} in kPa. Values of $\hat{u}_{lv}$ were determined using the following linear fit to data for water between 10°C and 70°C:

$$\hat{u}_{lv} = 7.016 \times 10^{-20}[1 - (T_d - 283.2)/825.4] \quad (10)$$

where $\hat{u}_{lv}$ is in J molecule^{-1} and T_d is in K. In the simulation, the summations of incident energy and number of incident non-condensable molecules were updated at each timestep. The droplet temperature was computed at each timestep by iteratively solving equations (8), (9) and (10) simultaneously. A guess of the surface temperature was provided to initiate the simulation. As the number of time steps increases, the surface temperature computed in this manner converges to a value which is interpreted as being the actual physical temperature of the droplet for the quasi-steady process being modeled in the simulation. This element of our simulation is distinctly different from that of Carey and Hawks [12] in which the surface temperature of the droplet was fixed at the saturation temperature for the pure fluid droplet at the system pressure.

Once the surface temperature of the droplet was determined for a given timestep, particles were computationally emitted from the droplet surface. First, N_{non} non-condensable particles were emitted, so that there is no net transfer of the non-condensable species to the droplet during the timestep. Then, particles of the condensable species were emitted from the droplet surface until an energy balance was achieved.

Each time a particle was emitted from the droplet surface, the energy carried away from the droplet by the particle was added to a cumulative total for the timestep. When this total just exceeded the amount delivered to the sphere during the timestep, the particle addition process was stopped. The amount by which the energy for the added particles exceeded that for the incoming particles was subtracted from the energy of the incoming particles in the next time step. This imposed a zero net energy flux condition on the droplet interface. However, the number of incident condensable particles exceeded the number of emitted condensable particles, resulting in a finite net mass flux to the droplet surface.

For both condensable and non-condensable particles, the location at which a particle is added to the simulation was determined by randomly sampling a distribution function which produces a uniform flux of particles over the spherical surface of the droplet. The velocity components and rotational energy were randomly sampled from appropriate Boltzmann distributions for molecules crossing a fixed surface in a gas at the specified sphere temperature T_d. The distributions used are described in the Appendix.

The energy of saturated water vapor molecules, on average, exceeds that of saturated liquid molecules by $\hat{u}_{lv}$. At temperature T_d, the mean energy of a water vapor molecule is $3k_B T_d$. The energy of an arbitrary water molecule in the gas with translational energy ε_{tr}

and rotational energy ε_{rot} thus exceeds the mean energy of the liquid water molecules in the droplet by $\varepsilon_{tr}+\varepsilon_{rot}-3k_B T_d+\hat{u}_{lv}$. In the energy balance calculations at the droplet interface, the mean energy of the saturated liquid molecules was taken as the level of zero energy for water molecules. The energy delivered to the droplet by one interacting water particle from the surrounding gas is therefore given by

$$\Delta E_{w,in} = N_{mpp}(\varepsilon_{tr}+\varepsilon_{rot}-3k_B T_d+\hat{u}_{lv}) \quad (11)$$

where N_{mpp} is the number of molecules per particle in the simulation. This relation was used to compute the energy delivered to the droplet by a water particle striking and interacting with the droplet. The energy delivered by one nitrogen particle is given by $N_{mpp}(\varepsilon_{tr}+\varepsilon_{rot})$. Based on similar reasoning, the following relation was used to compute the energy removed from the droplet by an emitted water particle

$$\Delta E_{w,em} = N_{mpp}(\varepsilon_{tr}+\varepsilon_{rot}-3k_B T_d+\hat{u}_{lv}) \quad (12)$$

where ε_{tr} and ε_{rot} were obtained by sampling the appropriate Boltzmann distributions at T_d.

In the simulation calculations in this study, the simulation domain shown in Fig. 1 was filled with cubic cells which formed a uniform Cartesian mesh. The radius of the droplet in the simulations ranged from 0.2 to 2.0 μm. The effects of cell and timestep sizes on the results of the simulation were explored and consequently the cell size was chosen to be on the order of one mean free path. The time step was chosen so a particle with average speed traveled approximately half a mean free path in one timestep. Generally, we found that the results were insensitive to the choice of these parameters as long as they were close to the values indicated by these guidelines. The side of the cell varied from 0.05 μm for the smallest droplets to 0.25 μm for the largest droplets considered in this study. The number of cells used was a compromise between accuracy and computational effort. The ratio of the number of molecules per particle N_{mpp} was chosen in each simulation to compromise between computational accuracy and storage limitations on the computer. The values used in the calculations reported here ranged from 1.78 to 1784 molecules per particle. Simulations were typically run for 16000 to 24000 timesteps, with a timestep typically being 200 ps.

After running the simulation for a sufficiently long time, the simulation predicts the equilibrium temperature and concentration fields adjacent to the surface of the droplet for arbitrarily specified values of the ambient pressure and the temperature and water vapor concentration at $r = 4r_d$. The matching procedure mentioned above was then used to determine the corresponding values of the temperature and water vapor concentration in the far ambient. To do so, the net heat flux from the droplet surface (carrying away the latent heat of the net condensation effect) is first computed from the simulation results using the following relation:

$$q''_d = \frac{\Delta N_{net}\hat{u}_{lv}N_{mpp}}{(4\pi r_d^2/8)N_{steps}\Delta t} \quad (13)$$

where N_{steps} is the number of timesteps in the simulation and ΔN_{net} is the net number of water particles transferred to the droplet due to particle interactions during the simulation to that timestep. Conservation of energy requires that a steady state, the heat flux through the spherical surface at $r/r_d = 4$ must be given by

$$q''_4 = (4)^{-2}q''_d = q''_d/16. \quad (14)$$

Transport of energy beyond $r = 4r_d$ is treated as continuum transport from an evaporating sphere with radius $4r_d$ for a surface temperature of T_4 and a heat flux of q''_4. The outward velocity due to the net generation of molecules at the droplet surface is negligible at $r = 4r_d$ and transport in the outer continuum region is, to a good approximation, by conduction only. It follows from the well known continuum solution for steady conduction from a sphere that

$$T_\infty = T_4 + \frac{r_d q''_d}{4k_v}. \quad (15)$$

Equations (13) and (15) were used to determine the ambient temperature T_∞. A completely analogous analysis of mass diffusion allows matching of the particle simulation to a continuum concentration field in the region beyond $r = 4r_d$. Following the same line of analysis as for the conduction heat transfer yields the following relations for the net mass flux of water vapor at the droplet surface m''_d and the ambient water vapor concentration $X_{w,\infty}$:

$$m''_d = \frac{\Delta N_{net}N_{mpp}}{(4\pi r_d^2/8)N_{steps}\Delta t} \quad (16)$$

$$X_{w,\infty} = X_{w,4} + \frac{r_d m''_d}{4\rho_v D_v}. \quad (17)$$

When required, the thermal conductivity of the mixture was computed using the method of Mason and Saxena [19] and the diffusion coefficient for water vapor was determined using the empirical correlation of Wilke and Lee [20]. Using the result of equation (16), the growth rate of the droplet can be computed as

$$\frac{dr_d}{dt} = \frac{m''_d}{\rho_l}. \quad (18)$$

To evaluate the simulation methodology described above, we compared predictions of the simulation method with recent experimental results from the literature. This comparison is described in the next section.

SIMULATION PREDICTIONS FOR ARGON–WATER MIXTURES

In a recent study, Peters and Paikert [21] experimentally determined the variation of water microdroplet size with time for droplets in supersaturated and superheated gas mixtures in a shock tube apparatus. These experiments produced a low volume concentration of virtually monodisperse droplets which grew through condensation while the gas was supersaturated and decreased in size when the gas was superheated. In this study, the intensity of scattered laser light was analyzed using Mie scattering theory to determine the variation of radius with time. These investigators presented plots of the measured radius versus time for droplet growth in water–argon mixtures. To evaluate the molecular simulation scheme described above, we determined the mean growth rate of the droplet between successive measured points in the Peters and Paikert [21] data and compared the values to the simulation predictions for the same conditions.

To conduct the comparison described above, it is necessary to choose a value of the thermal accommodation coefficient for use in the simulation. The value of the accommodation coefficient σ_t for a condensing or evaporating interface has been the subject of much debate. The tabulation assembled by Paul [22] lists values ranging from 0.02 to 0.04 for some liquids to values very near 1.0 for others. Mills [23] has suggested that molecular accommodation should be imperfect only when the interface is impure. Paul [22] notes that in almost every case where σ_t was found to be appreciably less than one, the average condition of the vapor molecules was different from that for the liquid phase because of association, disassociation or polymerization. This suggests that if the water in this study is assumed to be virtually pure and that association, disassociation and polymerization do not occur to any significant degree, the accommodation coefficient should be close to unity. On the other hand, recent deterministic molecular simulation studies by Yasuoka *et al.* [24] imply that the accommodation coefficient for a pure water interface should be near 0.4. In the analysis of their data, Peters and Paikert [21] suggested a value of 1.0 for the accommodation coefficient as best fitting their data in an analytical kinetic-theory model.

Based on these observations we performed simulation calculations for $\sigma_t = 0.5$ and 1.0 at the conditions of the experiment of Peters and Paikert [21]. These predictions are compared to the growth rates determined from the experimental data in Fig. 2. Also shown in Fig. 2 is the prediction of standard continuum theory using Fourier's law and Fick's law to predict the simultaneous heat and mass transfer associated with quasi-steady condensation at the indicated conditions. For the continuum model, the governing equation and boundary conditions are

$$r^{-2}\frac{\mathrm{d}}{\mathrm{d}r}(r^2 u_r) = 0 \tag{19}$$

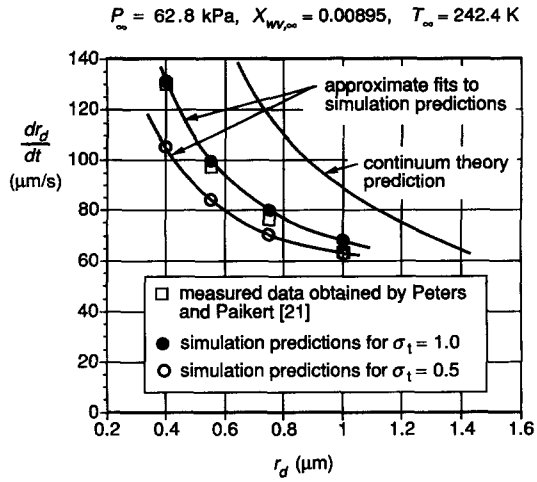

Fig. 2. Comparison of simulation predictions and continuum theory with droplet growth rates determined from the data of Peters and Paikert [21] for a water–argon mixture.

$$u_r\frac{\mathrm{d}u_r}{\mathrm{d}r} = -\frac{1}{\rho_v}\frac{\mathrm{d}P}{\mathrm{d}r} + \left(\frac{v_v}{r^2}\right)\frac{\mathrm{d}}{\mathrm{d}r}\left(r^2\frac{\mathrm{d}u_r}{\mathrm{d}r}\right) - \left(\frac{2v_v u_r}{r^2}\right) \tag{20}$$

$$\rho_v c_p u_r\frac{\mathrm{d}T}{\mathrm{d}r} = r^{-2}\frac{\mathrm{d}}{\mathrm{d}r}\left(r^2 k_v\frac{\mathrm{d}T}{\mathrm{d}r}\right) \tag{21}$$

$$u_r\frac{\mathrm{d}X_w}{\mathrm{d}r} = r^{-2}\frac{\mathrm{d}}{\mathrm{d}r}\left(r^2 D_v\frac{\mathrm{d}X_w}{\mathrm{d}r}\right) \tag{22}$$

$$r = r_d : u_r = -\left(\frac{k_v}{\rho_v h_{lv}}\right)\left(\frac{\mathrm{d}T}{\mathrm{d}r}\right)_{r=r_s} \quad T = T_{sat}(X_w P_\infty, r_d) \tag{23}$$

$$r \to \infty : u_r \to 0 \quad T \to T_\infty \quad X_w \to X_{w,\infty}. \tag{24}$$

Equations (19)–(22) represent conservation of total mass, momentum, energy and water vapor, respectively. In this formulation, $T_{sat}(X_w P_\infty, r_d)$ is the saturation temperature of water at the partial pressure $X_w P_\infty$, corrected for the effect of surface tension at the droplet radius r_d. For these circumstances, the continuity equation (19) dictates that the radial velocity decays from its value at the droplet surface proportional to r^{-2}. The continuity, water vapor transport and energy transport equations can be solved together with the boundary conditions to obtain the velocity, concentration and temperature fields. The momentum equation can then be solved for the pressure field if desired. The continuum analysis used here is similar to that described by Mills [25] for evaporating droplets, with the thermal conductivity and diffusivity evaluated using the methods described by Mason and Saxena [19] and Wilke and Lee [20]. The above system of equations and boundary conditions was solved to produce the continuum curve indicated in Fig. 2.

Overall, the simulation predictions in Fig. 2 for an accommodation coefficient close to unity provide a better fit to the experimentally determined values than

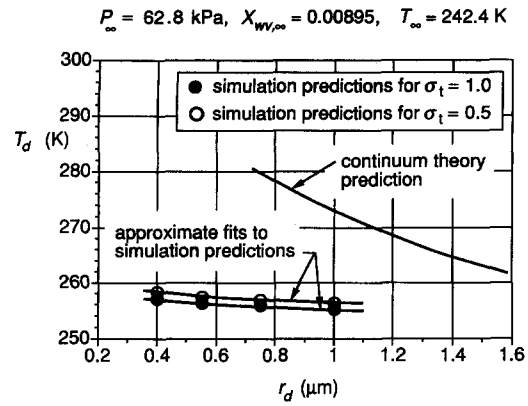

Fig. 3. Continuum theory and simulation predictions of the variation of T_d for the droplet growth conditions in the experiment of Peters and Paikert [21].

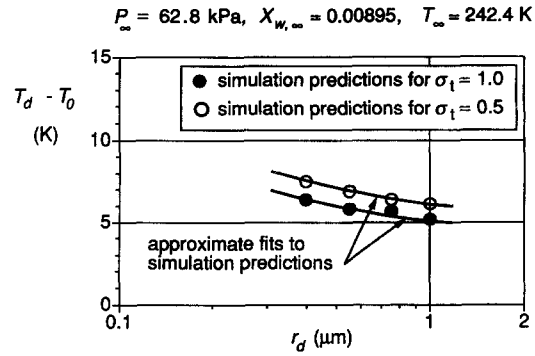

Fig. 4. Simulation predictions of the variation of temperature slip at the droplet surface for growth conditions in the experiment of Peters and Paikert [21].

the predictions for $\sigma_t = 0.5$. As expected, the difference between the simulation results for $\sigma_t = 1.0$ and $\sigma_t = 0.5$ increases as the droplet size decreases and non-continuum effects become larger. However, over the range of conditions considered here, the difference between the growth rate for $\sigma_t = 1.0$ and $\sigma_t = 0.5$ is less than 30%. For the ambient conditions represented in Fig. 2, radius values from 0.4 to 1.0 μm correspond to Knudsen numbers $Kn_D = \lambda_\infty/2r_d$ between 0.114 and 0.045. The data and the simulation predictions are both substantially lower than the continuum prediction, which is consistent with the expected behavior for Knudsen numbers above 0.02.

As part of our investigation we also examined other microscale features of the droplet growth process predicted by the simulation for the experimental conditions of Peters and Paikert [21]. Simulation predictions of the droplet temperature at different droplet radii are shown in Fig. 3 for $\sigma_t = 1.0$ and $\sigma_t = 0.5$. The droplet temperature at a given radius changes only slightly with accommodation coefficient between 0.5 and 1.0. Also shown is the droplet temperature variation predicted by the continuum model for comparable conditions. The simulation predictions are seen to be significantly lower than the corresponding simulation predictions.

The variation of the temperature slip at the droplet surface predicted by the simulation for the conditions in the Peters and Paikert [21] experiment is shown in Fig. 4 for $\sigma_t = 1.0$ and $\sigma_t = 0.5$. As expected, the slip decreases towards zero as the droplet size increases and the transport approaches continuum behavior. For this range of conditions, the slip varies only slightly for σ_t between 0.5 and 1.0.

The temperature and concentration profiles near the droplet predicted by the simulation for a 0.4 μm radius droplet under the conditions in Peters and Paikert's [21] experiment are shown in Fig. 5. The profiles shown in this figure were computed for $\sigma_t = 1.0$. These profiles exhibit the expected asymptotic approach to the ambient temperature and concentration at large r.

SIMULATION PREDICTIONS FOR NITROGEN–WATER MIXTURES

To further explore the interaction of vapor condensation and non-continuum effects, the simulation methodology described above was also applied to liquid microdroplets undergoing condensation growth in a supersaturated mixture of water vapor and nitrogen gas at a pressure of 19.94 kPa. The ambient temperature in these simulation calculations was approximately 250 K, which corresponds to an ambient of metastable supersaturated vapor below the freezing point of water. As will be seen, the temperature of the droplets for these conditions was generally above freezing, resulting in liquid droplet growth. This mixture combination and conditions were chosen because they are very similar to conditions encountered in the earth's atmosphere at high altitudes.

The observations in the previous section indicate that although there is some uncertainty associated with the appropriate value of accommodation coefficient, it is likely to lie between 0.4 and 1.0. We therefore selected $\sigma_t = 0.9$ as a representative value for the exploratory calculations for water–nitrogen mixtures presented here. Use of this value embodies the implicit assumptions that the liquid water is virtually pure and that association, disassociation and polymerization do not occur to any significant degree. The simulation scheme can, of course, be used with other accommodation coefficients for systems in which other values of σ_t are appropriate.

Simulation calculations for nitrogen–water gas mixtures presented here span ambient concentration levels ranging from 0.05 to 0.9999 and droplet radius values ranging from 0.2 to 2.0 μm. For the ambient conditions considered here, thermodynamic analysis indicates that the critical droplet radius above which an embryo will spontaneously grow is on the order of a few nm (see Carey [26]). Growth rate trends predicted by our simulation indicate that it would take only a few ms for a droplet of critical size to grow to a size of about 0.2 μm. Thus, the range of droplet radii considered here corresponds to the very early stages of the post-nucleation growth process.

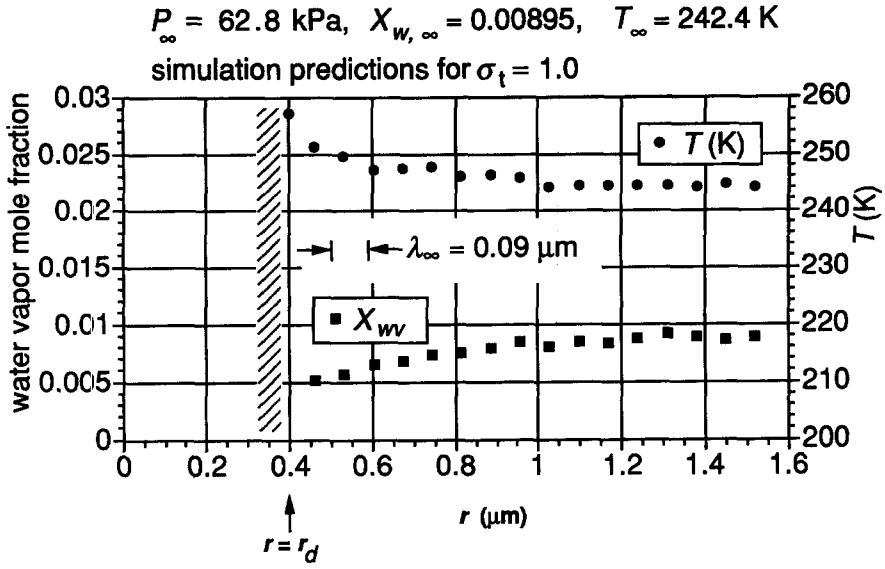

Fig. 5. Simulation prediction of the concentration and temperature profiles near the droplet at a radius of 0.4 μm for the growth conditions in the experiment of Peters and Paikert [21].

Figures 6–10 indicate the effect of varying ambient concentration on transport for a droplet with a radius of 1 μm for an ambient pressure of 19.94 kPa. Figure 6 shows the predicted variation of the droplet temperature with ambient water vapor concentration for ambient temperatures close to 250 K. The ambient temperature for each computed point is slightly different because in each case the computed ambient temperature determined by matching to the outer continuum solution was slightly different. Because the deviation of the ambient temperature from 250 K is generally small compared to the overall driving temperature difference $T_d - T_\infty$, the trends in the results are essentially the same as for a fixed ambient temperature of 250 K. Note that all the droplet temperatures are above freezing due to the temperature difference that is established by the release of latent heat at the droplet interface during condensation. Figure

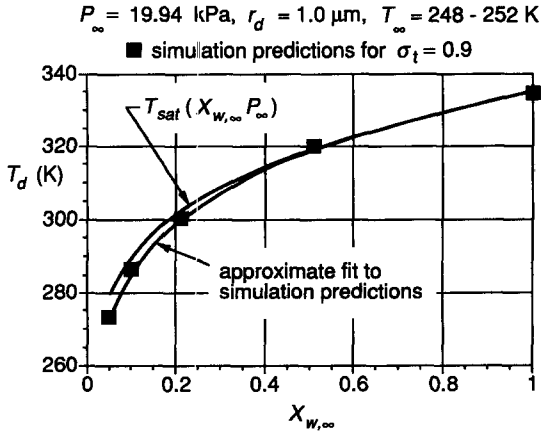

Fig. 6. Variation of T_d with ambient concentration for a droplet radius of 1 μm in water–nitrogen mixtures.

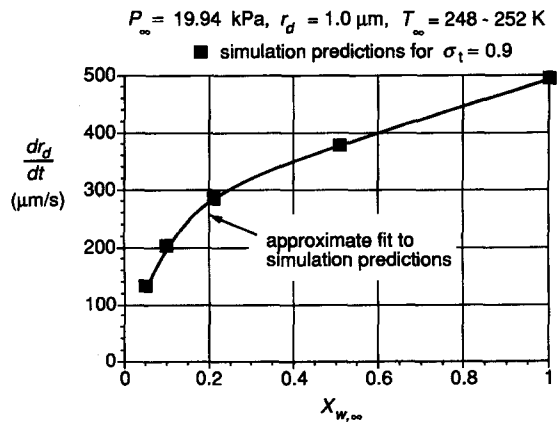

Fig. 7. Variation of droplet growth rate with ambient concentration for a droplet radius of 1 μm in water–nitrogen mixtures.

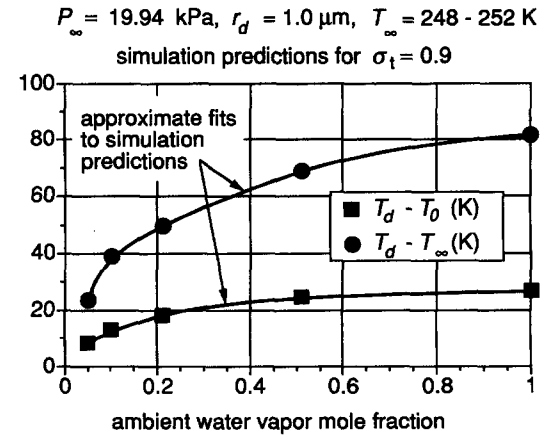

Fig. 8. Variation of temperature slip at the droplet surface and the overall temperature difference with ambient concentration for a droplet radius of 1 μm in water–nitrogen mixtures.

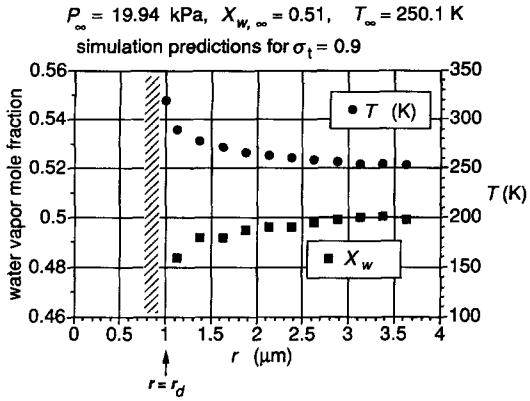

Fig. 9. Temperature and concentration profiles at $X_w = 0.51$ for a droplet radius of 1 μm in a water–nitrogen mixture.

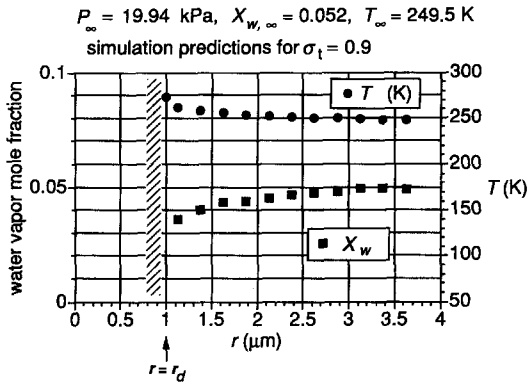

Fig. 10. Temperature and concentration profiles at $X_w = 0.052$ for a droplet radius of 1 μm in a water–nitrogen mixture.

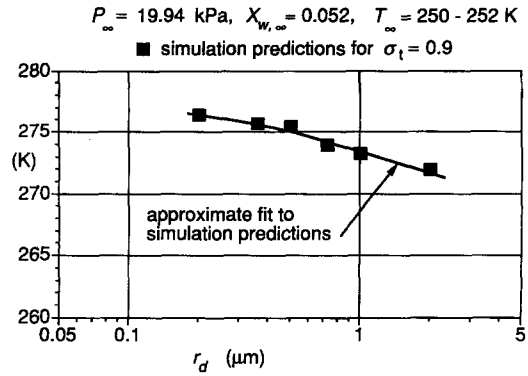

Fig. 11. Variation of T_d with droplet radius in a water–nitrogen mixture.

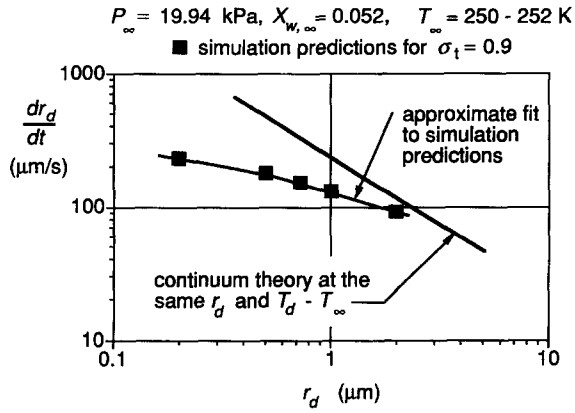

Fig. 12. Continuum theory and simulation predictions of the variation of droplet growth rate with droplet radius in a water–nitrogen mixture.

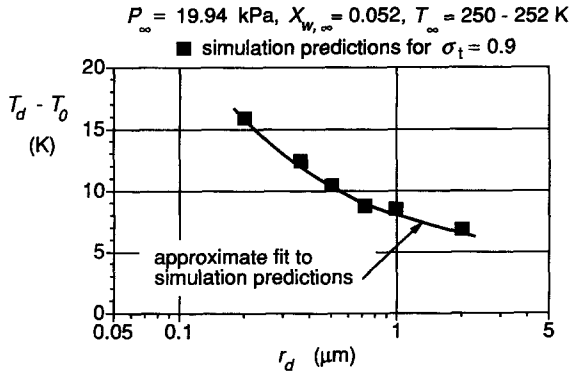

Fig. 13. Variation of temperature slip at the droplet surface with droplet radius in a water–nitrogen mixture.

6 shows a plot of the predicted variation of droplet temperature with ambient concentration. At each concentration, the droplet temperature is slightly below the saturation temperature of water at the ambient partial pressure of water vapor $X_{w,\infty}P_\infty$. As expected, the droplet temperature tends towards the pure water saturation temperature of 333 K as the ambient water mole fraction approaches 1.0.

The variation of the droplet growth rate with concentration is shown in Fig. 7. The growth rate decreases rapidly as the ambient concentration of water vapor decreases. The decrease in growth rate results from increased mass diffusion resistance and reduced driving temperature difference associated with lower water vapor concentration. Figure 8 shows the variation of overall driving temperature difference and temperature slip at the interface with ambient concentration. In absolute terms the slip at the interface increases with concentration, but as a fraction of the overall temperature difference, it actually decreases.

Figures 9 and 10 show the temperature and concentration profiles near the droplet for ambient water vapor mole fractions of 0.51 and 0.052, respectively. The temperature indicated at $r = r_d$ is the droplet surface temperature iteratively determined in the simulation. In both cases, the temperature profiles reflect the temperature slip at the interface. At both ambient concentrations, the concentration profiles indicate a significant reduction in water vapor concentration near the interface due to condensation on the droplet.

Figures 11–13 indicate the effect of varying droplet radius on transport for a droplet in a nitrogen–water mixture with an ambient pressure of 19.94 kPa, an ambient concentration of 0.052 and an ambient temperature near 251 K. As discussed above, the ambient

temperature values deviated slightly from 251 K due to slightly different results of matching to the continuum solution beyond $r = 4r_d$ and the deviation is small compared to the overall driving temperature difference. Figure 11 shows the predicted variation of the droplet temperature with droplet radius for quasi-static growth. These results clearly suggest that the droplet temperature decreases slightly as the droplet grows. This is consistent with the trends in Fig. 3 for the water–argon mixture in the experiment of Peters and Paikert [21]. The simulation predicted rate of droplet growth decreases with increasing size, as indicated in Fig. 12. Figure 12 also shows the prediction of continuum theory for the same variations of driving temperature difference and droplet radius as the simulation prediction points in this figure. It can be seen that the growth rates are below the continuum prediction, but approach it as the radius becomes larger. The simulation prediction of the variation of temperature slip at the droplet surface with droplet radius is shown in Fig. 13. Figures 12 and 13 indicate that the growth rate and temperature slip both decrease as the droplet grows.

In their study of evaporation of liquid nitrogen microdroplets in pure nitrogen vapor, Carey and Hawks [12] found that at high droplet evaporation rates the simulation predicted molecular velocity and rotational energy distributions that differed significantly from Boltzmann distributions near the droplet surface. This motivated us to examine these distributions near the condensing droplet in the simulations in this study. We therefore collected velocity component and rotational energy samples for water and nitrogen particles in the cell just outside a 1 μm radius droplet for $X_{w,\infty} = 0.51$, $T_\infty = 250.1$ K, $P_\infty = 19.94$ kPa. The velocity samples were then sorted in bins with size $0.05\sqrt{k_B T/m}$, where T is the local gas temperature in the cell and m is the molecular mass of the species of the particle. Note that this allows us to include particles of both species in the velocity distributions. The resulting velocity distributions are plotted in Fig. 14. Because water and nitrogen molecules obey different rotational energy distributions, the samples of rotational energy for these species were sorted separately into bins of size $0.1k_B T$, where T is the local temperature. The rotational energy distributions for water and nitrogen particles in the simulation near the droplet surface are compared with the corresponding Boltzmann distributions in Fig. 15.

Overall, there is close agreement between the sampled distributions and the Boltzmann distributions in Figs. 14 and 15. The scatter in the distributions is attributed to the limited number of samples that could be obtained in a reasonable computation time. The results indicate that this condensation driven droplet growth process does not give rise to distributions that deviate from equilibrium Boltzmann distributions, as was found by Carey and Hawks [12] for rapidly evaporating droplets in a superheated pure gas.

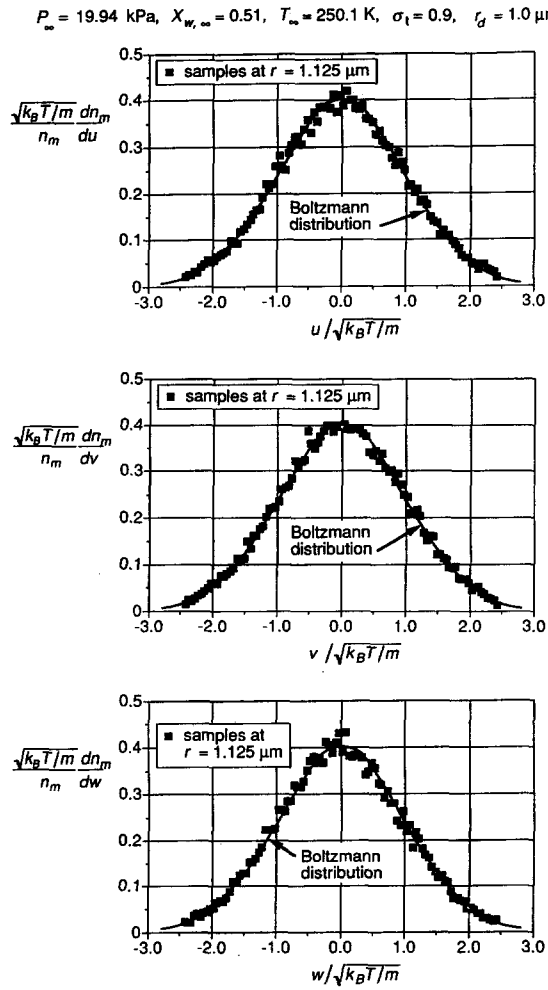

Fig. 14. Comparison of the u, v and w distributions in the simulation near the droplet with the Boltzmann distribution for a water droplet in a water–nitrogen mixture.

CONCLUDING REMARKS

This study explored the use of a direct simulation Monte Carlo technique to predict the transport during post-nucleation quasi-equilibrium growth of water microdroplets in supersaturated gas mixtures. The simulation employed a new treatment of the droplet interface boundary condition which makes it possible to compute the droplet surface temperature as part of the simulation calculation. This appears to be the first time such an interface model has been employed in a simulation scheme to model transport near a droplet undergoing condensation growth. The calculated results presented in this paper have demonstrated that this simulation method can be used to directly calculate the droplet surface temperature and the temperature and concentration profiles in the region adjacent to the droplet and the overall thermal energy transfer to the droplet during the condensation process.

The predictions of this scheme were found to be in close agreement with expected droplet condensation

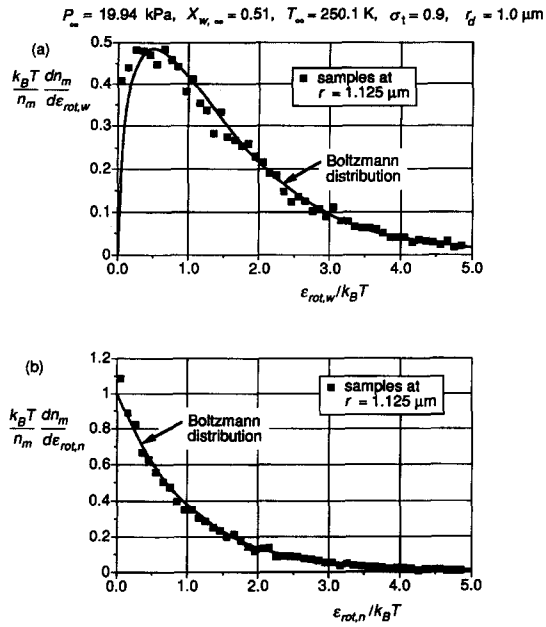

Fig. 15. Comparison of the rotational energy distributions in the simulation near the droplet with the Boltzmann distribution for a water droplet in a water–nitrogen mixture: (a) water molecules, (b) nitrogen molecules.

temperatures in the limit of water vapor concentration approaching unity. The simulation predictions for a water–argon mixture at an accommodation coefficient of about 1.0 were also found to agree well with droplet growth rates determined from an experiment by Peters and Paikert [21]. Peters and Paikert [21] found that their data agreed well with the droplet growth predicted by a modified form of the theoretical model developed by Young [10] for $\sigma_t = 1.0$. The good agreement between our simulation results for $\sigma_t = 1.0$ and the data of Peters and Paikert [21] thus implies that our results are also consistent with the predictions of the theory developed by Young [10]. While the close agreement of our results with the data of Peters and Paikert [21] does not completely validate the simulation methodology developed in this study, the fact that the predictions agree well with the experimental results is a first step towards establishing the viability of this model as a tool for predicting transport under conditions similar to those explored in this study.

Example calculations presented in this paper provide considerable insight into the transport associated with microdroplet evaporation in the transition regime. As expected, condensation of water vapor at the droplet surface reduces the water vapor concentration there below that in the ambient. The percentage change in water vapor concentration is small at moderate to high ambient concentration levels, but is very significant at low ambient concentration levels.

The results of this study indicate that non-continuum effects, and strong mass diffusion effects play important roles in the transport associated with quasi-equilibrium post-nucleation growth of water microdroplets in water–argon and water–nitrogen gas mixtures. These features of the transport were found to have a significant impact on the predicted droplet temperature. This implies that for circumstances of this type, the droplet temperature may, in general, depend on non-continuum effects and transport in the gas as well as the thermodynamic characteristics of the system. The non-continuum behavior at the surface can result in significant temperature slip in the gas adjacent to the interface and the gas mixture there is in a metastable supersaturated state. Nevertheless, our simulation results imply that the translation and rotational energy distributions of the molecules are consistent with equilibrium Boltzmann statistics at the local conditions. In contrast, Carey and Hawks [12] found that this was not the case for rapid evaporation of microdroplets in a superheated gas. These results clearly indicate that theoretical treatments of this type of transport problem must have the capability to handle these complexities if they are to provide accurate predictions of the droplet growth rates.

Acknowledgements—Support for this research was provided by the National Science Foundation under grant no. CTS-9024862 and Sandia National Laboratories.

REFERENCES

1. S-W. Kang, Analysis of condensation droplet growth in rarefied and continuum environments, *AIAA J.* **5**, 1288–1295 (1967).
2. R. E. Sampson and G. S. Springer, Condensation on and evaporation from droplets by the moment method, *J. Fluid Mech.* **36**, 577–584 (1969).
3. P. N. Shankar, A kinetic theory of steady condensation, *J. Fluid Mech.* **40**, 385–400 (1970).
4. P. Gajewski, A. Kulicki, A. Wisniewski and M. Zgorzelski, Kinetic theory approach to the vapour phase phenomena in non-equilibrium condensation process, *Physics Fluids* **17**, 321—327 (1974).
5. Y. S. Lou, On the nonlinear droplet condensation and evaporation problem, *J. Appl. Phys.* **49**, 2350–2356 (1978).
6. S. K. Loyalka, Condensation on a spherical droplet, II, *J. Colloid Interface Sci.* **87**, 216–224 (1982).
7. H. Lang, Heat and mass exchange of a droplet in a polyatomic gas, *Physics Fluids* **26**, 2109–2114 (1983).
8. V. G. Chernyak and A. Y. Margilevskiy, The kinetic theory of heat and mass transfer from a spherical particle in a rarefied gas, *Int. J. Heat Mass Transfer* **32**, 2127–2134 (1989).
9. J. B. Young, The condensation and evaporation of liquid droplets in a pure vapour at arbitrary Knudsen number, *Int. J. Heat Mass Transfer* **34**, 1649–1661 (1991).
10. J. B. Young, The condensation and evaporation of liquid droplets at arbitrary Knudsen number in the presence of an inert gas, *Int. J. Heat Mass Transfer* **36**, 2941–2956 (1993).
11. M. E. Widder and U. M. Titulaer, Kinetic boundary layers in gas mixtures: systems described by nonlinearly coupled kinetic and hydrodynamic equations and applications to droplet condensation and evaporation, *J. Stat. Phys.* **70**, 1255–1279 (1993).
12. V. P. Carey and N. E. Hawks, Stochastic modeling of molecular transport to an evaporating microdroplet in a superheated gas, *ASME J. Heat Transfer* **117**, 432–439 (1995).
13. M. M. El-Afify and M. L. Corradini, Transient con-

densation of vapor using a direct simulation Monte Carlo method, *Fusion Techn.* **15**, 783–790 (1989).
14. M. M. El-Afify and M. L. Corradini, Condensation of vapor in the presence of a noncondensable gas at low pressures, *Nucl. Engng Des.* **121**, 103–111 (1990).
15. G. A. Bird, *Molecular Gas Dynamics and the Direct Simulation of Gas Flows*. Oxford University Press, Oxford, U.K. (1994).
16. J. D. McDonald, A computationally efficient particle simulation method suited to vector computer architectures, Report SUDAAR 589, Department of Aeronautics and Astronautics, Stanford University (1989).
17. D. Baganoff and J. D. McDonald, A collision-selection rule for a particle simulation method suited to vector computers, *Physics Fluids A* **2**, 1248–1259 (1990).
18. I. Langmuir, The dissociation of hydrogen into atoms—II, *J. Am. Chem. Soc.* **37**, 417–458 (1915).
19. E. A. Mason and S. C. Saxena, Approximate formula for the thermal conductivity of gas mixtures, *Physics Fluids* **1**, 361–369 (1958).
20. C. R. Wilke and C. Y. Lee, Estimation of diffusion coefficients for gases and vapors, *Ind. Engng Chem.* **47**, 1253–1257 (1955).
21. F. Peters and B. Paikert, Measurement and interpretation of growth and evaporation of monodispersed droplets in a shock tube, *Int. J. Heat Mass Transfer* **37**, 293–302 (1994).
22. B. Paul, Compilation of evaporation coefficients, *ARS Journal* **32**, 1321–1328 (1962).
23. A. F. Mills, The condensation of steam at low pressures, Technical Report NSF GP-2520, series no. 6, issue no. 39, Space Sciences Laboratory, University of California at Berkeley (1965).
24. K. Yasuoka, M. Matsumoto and Y. Kataoka, Molecular simulation of evaporation and condensation. I. Self condensation and molecular exchange, *Proc. ASME/JSME Thermal Engineering Joint Conf.*, Volume 2, pp. 459–464 (1995).
25. A. F. Mills, *Heat and Mass Transfer*, Chaps. 9 and 10. Richard D. Irwin, Chicago, IL (1995).
26. V. P. Carey, *Liquid–Vapor Phase Change Phenomena*, Taylor and Francis, New York, NY (1992).
27. C. Borgnakke and P. S. Larsen, Statistical collision model for Monte Carlo simulation of a polyatomic gas mixture, *J. Computat. Phys.* **18**, 405–420 (1975).

APPENDIX

To initiate the particle simulation calculation, the cells in the simulation domain are initially loaded with particles, each of which represent a fixed number of molecules of a given type. The number of particles initially loaded into the cells is arbitrarily set to correspond to the ambient number density of molecules. The mean number of particles in each cell is subsequently determined as the calculation is marched forward in time.

The particles initially loaded into the cells are randomly given translational and internal (rotational) energies by randomly sampling values from the Boltzmann distribution for the gas (at equilibrium) at the outer boundary temperature. The particle simulation method marches the computation forward in time. For each time step Δt, the following operations were executed:

(1) Statistical information on particles in each cell was gathered at the beginning of each time step.
(2) All particles were transported in space at constant velocity along their current velocity vectors for time Δt, ignoring possible collisions.
(3) Each particle was checked to determine if it hit the droplet or hit a boundary of the simulation domain. If it had, appropriate actions were taken, based on the nature of the boundary. Specular surfaces only reverse the normal component of velocity of the particles that strike them. Particles striking the sphere or going beyond the outer boundary were removed from the simulation.
(4) Particles were randomly added to cells along the outer boundary surface $r = 4r_d$ to simulate the molecular flux (from the ambient) across this surface. The velocities and rotational energies were sampled from appropriate Boltzmann distributions for the outer boundary temperature.
(5) Particles were randomly added to cells along the droplet surface $r = r_d$ using the appropriate surface interaction model.
(6) Candidate collision pairs were randomly selected in each cell until approximately $n_p/2$ candidate collision pairs were formed per cell, where n_p is the particle number density in each cell. A selection rule (based on the statistical probability of collision) was used to determine whether the pair actually executed a collision.
(7) For each of the candidate pairs accepted for collision, the collision is executed, conserving energy and momentum. The orientation of the post-collision relative velocity vector was chosen randomly.

For particles added to the domain at the droplet surface or at the outer boundary, the surface normal velocity component ($c_\perp$) and the tangential velocity components ($c_=$) were sampled from the distributions

$$\mathfrak{I}(c_\perp)\,\mathrm{d}c_\perp = \frac{mc_\perp}{k_B T} e^{-mc_\perp^2/2k_B T}\,\mathrm{d}c_\perp \tag{A1}$$

$$\mathfrak{I}(c_=)\,\mathrm{d}c_= = \left(\frac{m}{2\pi k_B T}\right)^{1/2} e^{-mc_=^2/2k_B T}\,\mathrm{d}c_=. \tag{A2}$$

For diatomic nitrogen molecules, the rotational energy was sampled from

$$\mathfrak{I}(\varepsilon_{rot})\,\mathrm{d}\varepsilon_{rot} = \frac{1}{k_B T} e^{-\varepsilon_{rot}/2k_B T}\,\mathrm{d}\varepsilon_{rot} \tag{A3}$$

whereas for water, which is triatomic and non-linear, the rotational energy was sampled from

$$\mathfrak{I}(\varepsilon_{rot})\,\mathrm{d}\varepsilon_{rot} = \frac{2\varepsilon_{rot}^{1/2}}{\sqrt{\pi}(k_B T)^{3/2}} e^{-\varepsilon_{rot}/k_B T}\,\mathrm{d}\varepsilon_{rot}. \tag{A4}$$

In using the above distributions, T was set equal to either T_d or T_4, as appropriate. At the droplet surface $c_\perp$ was taken to be an outward normal velocity, whereas at the outer boundary it was taken to be an inward normal velocity. Sampled velocity components were subsequently converted to u, v and w components associated with the x–y–z coordinate system.

The selection rule used in step (6) above was essentially that recommended by Baganoff and McDonald [17]. For the hard sphere interaction model used in this study, this amounts to picking the number of potential collision pairs S for the cell equal to $\langle n_p\rangle/2$, where $\langle n_p\rangle$ is the mean particle number density in the cell, and selecting collision pairs with probability $\tilde{P}_s$ given by

$$\tilde{P}_s = 1.5\frac{\langle n_p\rangle |\mathbf{v}_r| \Delta t}{\sqrt{2}\bar{n}_{p,4}\lambda_4} \tag{A5}$$

where $\bar{n}_{p,4}$ and λ_4 are the mean particle density and mean free path for the reference condition at $r = 4r_d$, and $|\mathbf{v}_r|$ is the magnitude of the pre-collision relative velocity of the particles being considered as a possible collision pair. The value of the multiplier 1.5 in equation (A5) was chosen to match simulation collision frequencies with collision frequency predictions of kinetic theory for the conditions considered in this study.

Molecular collisions within the vapor were modeled with a simple hard sphere interaction model. For hard-sphere collisions, post-collision relative velocities must be iso-

tropically scattered. The method used in this study to randomly select post-collision velocities with isotropic scattering has been widely used in direct molecular simulation calculations. A detailed description of this methodology can be found in Bird [15] or McDonald [16].

If the collision is elastic (no exchange of energy in internal modes), the magnitude of the post-collision relative velocity vector is set equal to the value dictated by the pre-collision velocities of the particles. If the collision is inelastic, however, the post-collision fraction of relative translational energy to total collision energy is sampled from the distribution for an equilibrium gas. A relation for this fraction f_{rt} which is applicable to different molecular species with different intermolecular force potentials has been derived by Borgnakke and Larsen [27]. In the simulation scheme described in this paper, the molecules have a hard-sphere force interaction potential and have rotational internal storage only. The relation developed by Borgnakke and Larsen [27] then prescribes that f_{rt} obeys the distributions (A6), (A7) and (A8) below for nitrogen–nitrogen collisions, water–water collisions and nitrogen–water collisions, respectively,

$$\Im(f_{rt})\,\mathrm{d}f_{rt} = 6f_{rt}(1-f_{rt})\,\mathrm{d}f_{rt} \tag{A6}$$

$$\Im(f_{rt})\,\mathrm{d}f_{rt} = 12f_{rt}(1-f_{rt})^2\,\mathrm{d}f_{rt} \tag{A7}$$

$$\Im(f_{rt})\,\mathrm{d}f_{rt} = (35/4)f_{rt}(1-f_{rt})^{3/2}\,\mathrm{d}f_{rt}. \tag{A8}$$

In our calculations, the appropriate distribution for each type of molecular collision was randomly sampled to determine the f_{rt} value for each collision.

Following McDonald [16], an effective rotational collision number of 5 was used in our calculations with the result that one in five collisions was treated as inelastic. The method used to partition the collision energy in the post-collision state using the stochastically determined f_{rt} value is similar to that used by Carey and Hawks [12] for droplet evaporation in pure vapor and by McDonald [16] for high-speed rarefied gas flows.

In our simulation calculations, the post-collision partitioning of internal energy between the two molecules as assumed to obey the distribution relation cited by Bird [15] for f_{r1}, the fraction of the post collision internal energy allocated to molecule 1. For nitrogen–nitrogen collisions involving only rotational internal storage, the distribution function for the fraction of the internal energy allocated to molecule 1 is given by

$$\Im(f_{r1})\,\mathrm{d}f_{r1} = \mathrm{d}f_{r1}. \tag{A9}$$

The distribution for water–water collisions is similarly given by

$$\Im(f_{r1})\,\mathrm{d}f_{r1} = \left(\frac{8}{\pi}\right)f_{r1}^{1/2}(1-f_{r1})^{1/2}\,\mathrm{d}f_{r1}. \tag{A10}$$

For nitrogen–nitrogen or water–water collisions either molecule can be designated as molecule (1). For water–nitrogen collisions, the water molecule is designated as molecule 1 and the distribution for the fraction of the post collision energy allocated to the water molecule is given by

$$\Im(f_{r1})\,\mathrm{d}f_{r1} = (\tfrac{3}{2})f_{r1}^{1/2}\,\mathrm{d}f_{r1}. \tag{A11}$$

In our calculations, the appropriate distribution for each type of molecular collision was randomly sampled to determine the f_{r1} value for each collision.

To evaluate the mean free path for each species i in the mixture with the other species j, the following relation from kinetic theory was used

$$\lambda_i = [n_{m,j}(D_m)_{ii}^2\sqrt{2} + n_{m,j}(D_m)_{ij}^2\sqrt{1+m_i/m_j}]^{-1}. \tag{A12}$$

The mean free path for the mixtures was computed as a mole-fraction-weighted average

$$\lambda = X_w\lambda_w + (1-X_w)\lambda_n \tag{A13}$$

where λ_w and λ_n are the mean free path for water and nitrogen molecules, respectively, computed using equation (A12).